

## Angle-Resolved Photon-Stimulated Desorption of Oxygen Ions from a W(111) Surface

Theodore E. Madey and Roger Stockbauer

*Surface Science Division, National Bureau of Standards, Washington, D. C. 20234*

and

J. F. van der Veen and D. E. Eastman

*IBM Thomas J. Watson Research Center, Yorktown Heights, New York 10598*

(Received 15 April 1980)

A definitive determination of angle-resolved photon-stimulated desorption of ions from a well-characterized adsorbate, and a direct comparison with electron-stimulated desorption are reported. Ion angular distributions, energy distributions, and photon excitation spectra for  $O^+$  desorption from W(111) have been measured for oxygen coverages ranging from a fractional monolayer to a multilayer oxide.

PACS numbers: 68.45.Da, 68.20.+t, 79.90.+b

The electron-stimulated desorption (ESD) of ions from adsorbed layers on surfaces has been demonstrated to be a useful probe for studying adsorbate-substrate interactions.<sup>1,2</sup> Knotek and Feibelman<sup>3</sup> (KF) have proposed a core-hole Auger decay mechanism for ESD which predicts that ion desorption from ionically bonded species at surfaces is independent of the manner of production of the core hole, whether by electrons or photons. Recently, it has been shown<sup>4-7</sup> that photon stimulated desorption (PSD) of ions from surfaces does occur and that the threshold energies for ESD and PSD are similar and can often be associated with the production of core holes. One of the most useful aspects of ESD for surface characterization is the fact that ESD ion angular distribution (ESDIAD) measurements have been shown, for a variety of adsorbate-substrate systems, to provide information concerning the initial-state bonding geometry of adsorbed atoms and molecules.<sup>1,8</sup>

The objectives of the present PSD study of oxygen on W(111) were twofold. Firstly, we wished to determine whether or not the angular anisotropy of  $O^+$  ion emission observed in ESDIAD, i.e., discrete off-normal  $O^+$  beams,<sup>9,10</sup> would also be observed in PSD ion angular distributions. Secondly, we wished to examine the PSD of  $O^+$  from a W surface over a wide range of surface preparation conditions, ranging from a fractional monolayer of oxygen atoms to several monolayers of tungsten oxide. The basic question of interest concerns the nature of the adsorbed oxygen species which yield the ESD and PSD  $O^+$  signals: How do the mechanisms for  $O^+$  desorption from a monolayer and fractional monolayers of oxygen on W(111) compare with the  $O^+$  desorption mechanisms from tungsten oxide? That is, are

the  $O^+$ -yielding species in the monolayer characteristic of the majority of the adsorbed oxygen atoms,<sup>10</sup> or are they a minority state associated with oxidelike species<sup>1,11</sup> adsorbed at special sites (defects, steps)?<sup>1</sup>

We demonstrate that PSD and ESD ion angular distributions for  $O^+$  desorption from W(111) are identical, that the PSD threshold behavior is consistent with the KF Auger decay mechanism, and that the  $O^+$ -yielding species for monolayer coverages constitute a minority of the surface atoms. We also show that PSD of  $H^+$  from hydrogen adsorbed on the oxidized W surface proceeds via different excitations from those leading to  $O^+$  desorption. Finally, these data clearly indicate the potential of angle-resolved PSD for determining the bonding structures of adsorbed atoms and molecules, by selective excitation of surface species having different thresholds for ion desorption.

The experimental ultrahigh vacuum system used for these studies has been described in detail previously.<sup>6,12</sup> An ellipsoidal mirror analyzer with a microchannel plate detector was used to display the PSD and ESD angular patterns, as well as to measure the energy distributions of PSD ions or photoemitted electrons, the time-of-flight mass spectra of ions, and the Auger electron spectra of the sample surface. Photons in the energy range 8 to 120 eV were provided by the Tantalus II storage ring in conjunction with a toroidal grating monochromator. The W(111) sample crystal ( $6 \times 4 \times 0.7$  mm<sup>3</sup>) was cleaned by repeated oxidation, followed by flashing in vacuum to >2300 K. Oxygen coverages at 300 K were estimated from the coverage versus exposure data of Niehus,<sup>10</sup> and verified with Auger and photoelectron spectroscopies. The oxide surfaces

used herein were generated by heating at  $\sim 1000$  K at  $1 \times 10^{-6}$  Torr for 200 s, a procedure known to produce  $\geq 3$  monolayers of oxides on polycrystalline W surfaces.<sup>13</sup>

Figure 1 contains plots of the total  $O^+$  ion yield, corrected for photon flux, as a function of photon energy. Figure 1, curve *b* corresponds to the oxide surface, Fig. 1, curve *c* is the yield from an oxygen monolayer ( $15 \times 10^{-6}$  Torr s  $O_2$  at  $\sim 300$  K) and Fig. 1, curve *d* is the yield from  $\sim 0.5$  monolayer of oxygen ( $1.0 \times 10^{-6}$  Torr s  $O_2$ ). The ions were determined to be  $O^+$  by a time-of-flight method. The distinct "breaks" or onsets in the yield curves correspond roughly to the core-hole binding energies for tungsten atoms in solid W and in  $WO_3$  (Ref. 14) indicated on the figure. We note that Fig. 1, curve *c* is similar to PSD data for an oxygen monolayer on W(100).<sup>5</sup> Structure has also been seen in ESD ion yields of  $O^+$  from W(100).<sup>15</sup> Also of interest is the similarity be-

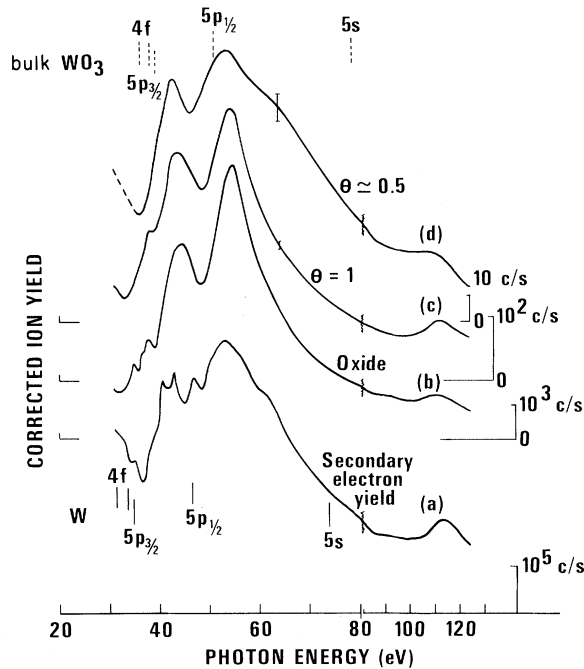


FIG. 1. Electron and ion yields for W(111) as a function of photon energy, corrected for monochromator transmission and second-order contributions. Ion yields are normalized to the same incident flux. Curve *a*, secondary electron yield at constant final state ( $E_{kin} = 3$  eV) for an oxygen monolayer. Curve *b*,  $O^+$  ion yield from an oxide layer. Curve *c*,  $O^+$  yield from an oxygen monolayer. Curve *d*,  $O^+$  yield from an 0.5 monolayer coverage. Binding energies for W core levels in pure W (solid lines) and  $WO_3$  (dashed lines) are shown. The energy scale changes at 80 eV.

tween the ion-yield curves and the secondary electron-yield curve of Fig. 1, curve *a* measured for the surface with an oxygen monolayer. Such a constant final-state (3-eV kinetic-energy electrons) plot of the secondary electron cascade has been shown<sup>16</sup> to be directly proportional to the soft x-ray absorption coefficient. Although most of the structure in Fig. 1, curve *a* is due to such inelastic processes, the sharp peaks at 40 and 43 eV are due to direct emission from W 4f levels. The PSD  $O^+$  ion yield for the oxide surface is estimated to be  $\sim 3 \times 10^{-8}$  ions/photon at  $h\nu = 55$  eV; the ESD ion yield for the same surface is  $\sim 1 \times 10^{-6}$  ions/electron at 500 eV.

The overall agreement between ion yields and the secondary electron yield indicates that photo-induced excitations of substrate W atoms play a major role in the desorption of ions, consistent with the KF model. The differences in detail are likely due to the fact that PSD ions originate only from the top layer of surface atoms for which the local density of states is different from that in bulk, whereas the secondary yield curve results largely from pure W metal. Note also that there is not a one-to-one correlation with the W core-level binding energies. Differences can be caused by the delayed onsets expected for high-angular-momentum states,<sup>17</sup> interference processes involving different final states,<sup>18</sup> and possible oxygen-induced chemical shifts in the surface W atoms.

The similarity of ion- and secondary-electron-yield curves suggests that ion desorption may be caused by secondary electrons, rather than by direct photon excitation. However, as shown previously<sup>5,7</sup> and verified in the present work, the number of emitted electrons having sufficient energy to cause ESD is two to three orders of magnitude smaller than necessary to account for the observed ion yield.

Note that all three ion-yield curves are dominated by peaks at  $\sim 45$  and 55 eV. This suggests that the  $O^+$ -yielding species for  $\theta > 1$ ,  $\theta \approx 1$  and the oxide layer have similar electronic configuration. The Auger decay model<sup>3</sup> of ion desorption requires maximal valency for the cationic species (i.e.,  $W^{6+}$  as in  $WO_3$ ); reduced forms of the oxide lead to little or no ion yield due to the increased valence-electron density on the cation, as in  $W^{4+}$ . Thus, we conclude that maximal valency species are present even in monolayers and fractional monolayers of oxygen. As indicated by the relative intensities of curves *a-c* in Fig. 1, such species must have a low concentration at

coverages  $\leq 1$  monolayer, and hence, ESD and PSD of  $O^+$  is due to a "minority species." It had been previously suggested<sup>10</sup> that the  $O^+$  seen in ESD of fractional monolayers of oxygen on W(111) was due to a majority of the adsorbed oxygen species, whereas the  $O^+$ -yielding sites on stepped surfaces vicinal to W(110) were shown to be minority sites,<sup>1</sup> i.e., steps and defects.

Figure 2 contains a sequence of PSD angular distribution patterns for the oxidized surface taken at different photon energies. The three  $O^+$  beams are symmetrically disposed about the normal, each having a polar angle  $\alpha$  of  $41^\circ \pm 2^\circ$  with respect to the normal. The value of  $\alpha$  depends on coverage and temperature, and is  $27^\circ \pm 3^\circ$  in the similar PSD pattern observed for monolayer oxygen at 300 K. The azimuthal orientation in Fig. 2 is in agreement with ESD of  $O^+$  from W(111).<sup>9,10</sup> Three other very faint beams desorbing with a larger polar angle and an azimuthal angle rotated by  $30^\circ$  are out of the field of view.<sup>9,10</sup> Note that the angular distributions are virtually identical at all energies, even though different substrate excitations are involved in each case. Thus, the final state appears to be the same irrespective of the initial-state excitation, consistent with the KF Auger decay mechanism. The present experiments indicate that the symmetry and angular separations of the PSD patterns are identical to those of the ESDIAD patterns excited by

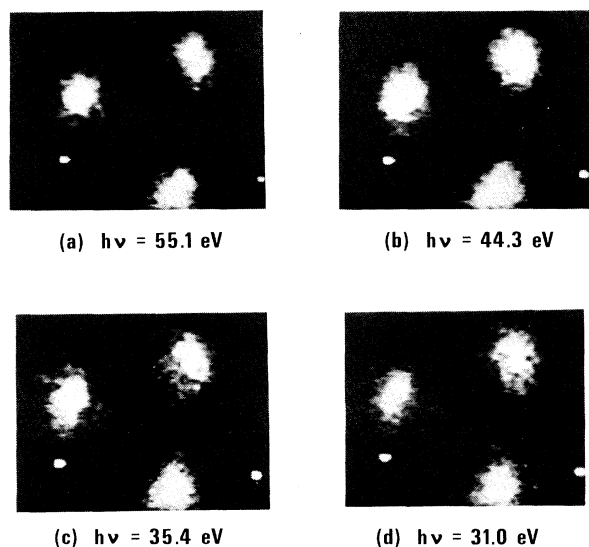


FIG. 2. PSD ion angular-distribution patterns for  $O^+$  desorption from the oxidized W(111) surface for different photon energies. The two small white dots are markers on the detector screen.

500-eV electrons.

Figures 3(a)–3(c) illustrate the  $O^+$  ion kinetic-energy distributions measured under different conditions with  $h\nu = 55$  eV. Peaks in the energy distributions are at  $\sim 8.5$  eV and the full widths at half maximum (FWHM) are  $\sim 2.8$  eV; where direct comparisons have been made, the energy distributions are the same for PSD and ESD (500-eV electrons). The angular distribution of one of the PSD  $O^+$  beams of Fig. 2 is plotted as Fig. 3(e). The FWHM is  $16^\circ$ , consistent with the thermal vibrational amplitudes expected for surface atoms.<sup>8</sup>

Finally, we note that PSD shows promise for studying minority species, molecular adsorbates, and coadsorbed species. For example, Fig. 3(d) depicts a PSD ion energy distribution observed after exposure of the oxidized surface to atomic hydrogen produced by dissociation of  $H_2$  on a hot W filament. With use of the time-of-flight method, the high kinetic-energy ions were identified as  $O^+$  (or  $OH^+$ ) and the low kinetic-energy ions as  $H^+$ . The PSD angular pattern for the  $O^+$  (or  $OH^+$ ) is similar to that for the "clean" oxide, with an intensity about  $\frac{1}{20}$  that of the "clean" oxide, i.e., the bonding of H to the surface inhibits  $O^+$  (or  $OH^+$ ) desorption. The PSD pattern for  $H^+$

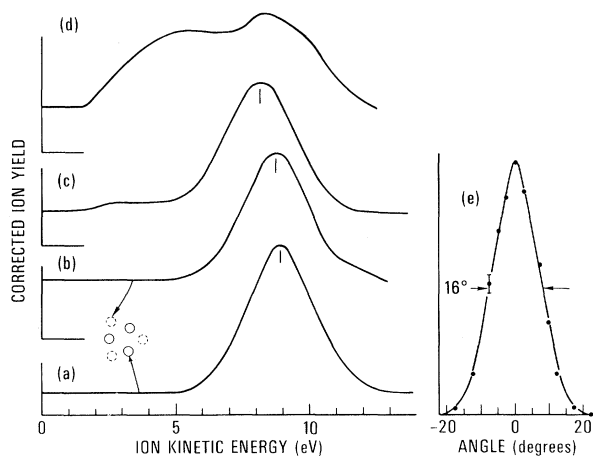


FIG. 3. Energy and angular distributions for PSD from W(111) under different conditions. (a) Energy distribution of  $O^+$  ions from the oxide layer, for the three inner beams (shown in Fig. 2). (b) Energy distribution for  $O^+$  from one of the outer beams of the oxide surface. (c)  $O^+$  desorption from monolayer. (d) Energy distribution of ions following exposure of the oxide to atomic H. (e) Angular profile of  $O^+$  ions for an inner beam from the oxide surface (cf. Fig. 2) for  $h\nu = 55$  eV.

is a triangular array with polar and azimuthal angles close to that of the  $O^+$  ( $OH^+$ ), suggesting a linear W-O-H species.<sup>19</sup> A photoexcitation spectrum for  $H^+$  shows the dominant threshold at  $\geq 20$  eV and a smaller threshold at  $\sim 37$  eV, whereas the  $O^+$  (or  $OH^+$ ) thresholds are similar to those in Fig. 1. This suggests that  $H^+$  desorption proceeds via excitation of a surface OH bond, perhaps by an O 2s core hole ( $\sim 22$  eV), and that W substrate excitations play a lesser role in  $H^+$  desorption.

The authors acknowledge valuable discussions with P. Heimann, M. Traum, N. Smith, M. Knotek, C. Olson, J. Weaver, and W. Clinton, and the support of E. M. Rowe and the staff of the University of Wisconsin Synchrotron Radiation Center. This work was supported in part by the Office of Naval Research.

<sup>1</sup>T. E. Madey and J. T. Yates, Jr., *Surf. Sci.* **63**, 203 (1977); T. E. Madey, *Surf. Sci.* **94**, 483 (1980).

<sup>2</sup>D. Menzel, in *Topics in Applied Physics*, edited by R. Gomer (Springer-Verlag, Berlin, 1975), Vol. 4, p. 101.

<sup>3</sup>M. L. Knotek and P. J. Feibelman, *Phys. Rev. Lett.* **40**, 964 (1978), and *Phys. Rev. B* **18**, 6531 (1978).

<sup>4</sup>M. L. Knotek, V. O. Jones, and V. Rehn, *Phys. Rev. Lett.* **43**, 300 (1979).

<sup>5</sup>D. P. Woodruff, M. M. Traum, H. H. Farrell, N. V. Smith, P. D. Johnson, D. A. King, R. L. Benbow, and Z. Hurych, *Phys. Rev. B* (to be published).

<sup>6</sup>J. F. Van der Veen, F. J. Himpsel, D. E. Eastman, and P. Heimann, to be published.

<sup>7</sup>R. Franchy and D. Menzel, *Phys. Rev. Lett.* **43**, 865 (1979).

<sup>8</sup>T. E. Madey, J. T. Yates, Jr., A. M. Bradshaw, and F. M. Hoffmann, *Surf. Sci.* **89**, 370 (1979); T. E. Madey and J. T. Yates, Jr., *Chem. Phys. Lett.* **51**, 77 (1977); T. E. Madey, *Surf. Sci.* **79**, 575 (1979).

<sup>9</sup>T. E. Madey, J. J. Czyzewski, and J. T. Yates, Jr., *Surf. Sci.* **57**, 580 (1976).

<sup>10</sup>H. Niehus, *Surf. Sci.* **87**, 561 (1979), and **80**, 245 (1979).

<sup>11</sup>T. Engel, H. Niehus, and E. Bauer, *Surf. Sci.* **52**, 237 (1975).

<sup>12</sup>D. E. Eastman, J. J. Donelon, N. C. Hien, and F. J. Himpsel, to be published.

<sup>13</sup>D. A. King, T. E. Madey, and J. T. Yates, Jr., *J. Chem. Phys.* **55**, 3247 (1971).

<sup>14</sup>G. Hollinger, T. Duc, and A. Deneuve, *Phys. Rev. Lett.* **37**, 1564 (1976).

<sup>15</sup>J. Kirschner, D. Menzel, and P. Staib, *Surf. Sci.* **87**, L267 (1979).

<sup>16</sup>W. Gudat and C. Kunz, *Phys. Rev. Lett.* **29**, 169 (1972); J. Stöhr, *J. Vac. Sci. Technol.* **16**, 37 (1979).

<sup>17</sup>J. H. Weaver and C. G. Olson, *Phys. Rev. B* **14**, 3251 (1976).

<sup>18</sup>L. C. Davis and L. A. Feldkamp, *Solid State Commun.* **19**, 413 (1976).

<sup>19</sup>S. Andersson and J. W. Davenport, *Solid State Commun.* **28**, 677 (1978).

## Pinning of Superfluid Vortices to Surfaces

S. G. Hegde and W. I. Glaberson

*Department of Physics, Rutgers University, Piscataway, New Jersey 08854*

(Received 10 April 1980)

The effect of surface roughening on the onset of vortex motion in thermal counterflow in a rotating channel has been investigated. Smooth surfaced channels exhibit a critical counterflow velocity independent of surface characteristics. Rough surfaced channels exhibit a larger critical velocity, larger by just the amount necessary to bring the average vorticity at the surface parallel to the surface.

PACS numbers: 67.40.Vs

Vortex pinning plays an important role in a variety of flow phenomena in superfluid helium. Vortex-wave resonance experiments,<sup>1-3</sup> involving oscillating disks or cylinders in a rotation field, depend on the pinning of vortices to the resonant cavity surfaces. It is believed<sup>4</sup> that a class of critical velocities for superflow through a channel involves an instability of pinned vortex lines.

The interpretation of the observed superfluid transition in thin helium films in terms of Kosterlitz-Thouless topological long-range order<sup>5</sup> depends crucially on the ability of thermally excited vortex-antivortex pairs to diffuse along the film. The nature of vortex pinning has not been well understood and, until recently, it was assumed<sup>6-8</sup> that vortices move along a superfluid-

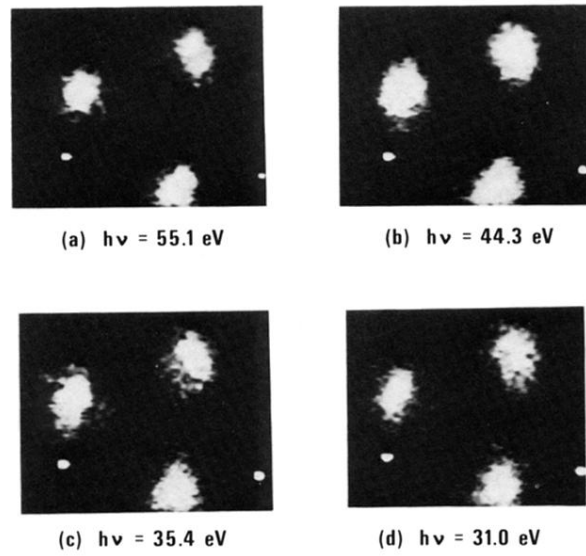


FIG. 2. PSD ion angular-distribution patterns for  $\text{O}^+$  desorption from the oxidized W(111) surface for different photon energies. The two small white dots are markers on the detector screen.